DR. BERN KOHLER (Orcid ID : 0000-0001-5353-1655)

Article type : Special Issue Research Article

Intermolecular Hydrogen Bonding Modulates O-H Photodissociation in Molecular Aggregates of a Catechol Derivative†

Christopher Grieco,[1] Forrest R. Kohl,[1] Yuyuan Zhang,[1] Sangeetha Natarajan,[1] Lluís Blancafort,[2*] Bern Kohler*[1]

[1]Department of Chemistry and Biochemistry, The Ohio State University, 100 West 18th Avenue, Columbus, Ohio 43210, USA

[2]Institut de Química Computacional i Catàlisi and Departament de Química, Universitat de Girona. Facultat de Ciències, C/M.A. Capmany 69, 17003 Girona, Spain.

*Corresponding authors' emails:

kohler@chemistry.ohio-state.edu (Bern Kohler)
lluis.blancafort@udg.edu (Lluís Blancafort)

†This article is part of a Special Issue celebrating Photochemistry and Photobiology's 55th Anniversary.

Abstract

The catechol functional group plays a major role in the chemical properties of a wide variety of molecules important in biology and technology. In eumelanin, intermolecular hydrogen bonding between these functional groups is thought to contribute to UV photoprotective and radical buffering properties, but the mechanisms are poorly understood. Here, aggregates of 4-*t*-butylcatechol are used as model systems to study how intermolecular hydrogen bonding influences photochemical pathways that may occur in eumelanin. Ultrafast UV-visible and mid-IR transient

absorption measurements are used to identify the photochemical processes of 4-*t*-butylcatechol monomers and their hydrogen-bonded aggregates in cyclohexane solution. Monomer photoexcitation results in hydrogen atom ejection to the solvent via homolytic O-H bond dissociation with a time constant of 12 ps, producing a neutral semiquinone radical with a lifetime greater than 1 ns. In contrast, intermolecular hydrogen bonding interactions within aggregates retard O-H bond photodissociation by over an order of magnitude in time. Excited state structural relaxation is proposed to slow O-H dissociation, allowing internal conversion to the ground state to occur in hundreds of picoseconds in competition with this channel. The semiquinone radicals formed in the aggregates exhibit spectral broadening of both their electronic and vibrational transitions.

Introduction

The catechol functional group plays a central role in the chemical properties of various biological and synthetic materials such as eumelanins (1-4), bioinspired adhesive polymers (5-8), and phenolic compounds present in fruit (9, 10) and wine (11, 12). Fruit browning (9, 10), the alteration of wine flavor (11, 12), and melanin synthesis (13, 4, 14) are all caused by oxidative reactions that form quinones or quinone-containing polymers from building blocks with 1,2-dihydroxybenzene (catechol) units. The catechol functional group also contributes to the photoprotective function of eumelanin materials (15), which are synthesized by oxidative polymerization of 5,6-dihydroxyindole. Furthermore, the proximity of the hydroxy groups enhances the stability of the semiquinone radical (16), and enables chelation with metals, such as iron, promoting cross-linking and self-healing in adhesive polymers (5-7, 4).

Intermolecular hydrogen-bonding interactions between catechol functional groups are central to some of the supramolecular motifs proposed to occur in eumelanins (17, 2, 3). Aggregated domains of dihydroxy-containing molecules play a photoprotective role in melanin chemistry (14), but the precise mechanisms remain elusive. Uncertainty about the chemical structures found in eumelanins and the likely presence of significant heterogeneity (1, 18, 15) complicate the interpretation of spectroscopic measurements (19-22). For these reasons, a number of investigators have studied simplified model systems containing chemical groups in arrangements thought to be present in eumelanin (20, 21, 23). These studies have addressed the impact of covalent bonding within dimers and oligomers in addition to solute-solvent interactions, but studies isolating the effects of intermolecular hydrogen-bonding interactions in aggregates are lacking to the best of our knowledge (18).

Here, we investigate the effects of intermolecular hydrogen bonding on UV-initiated photochemical and photophysical relaxation pathways in aggregates of 4-*t*-butylcatechol (4-tBuC, **Scheme 1**) as a step toward understanding photoprocesses in natural and synthetic eumelanins. This catechol derivative was chosen as an alternative to 5,6-dihydroxyindole and other eumelanin precursors because the latter compounds spontaneously oxidize in solution (22, 24). Our measurements were performed in cyclohexane solutions to isolate intermolecular hydrogen bonding from solute-solvent interactions. A *t*-butyl-substituted catechol was chosen because the alkyl side chain significantly enhances its solubility in cyclohexane. Horbury et al. (25) studied O-H bond photodissociation of monomeric 4-tBuC molecules in several solvents. Inspired by this work, our investigation seeks to understand how intermolecular hydrogen bonding interactions within 4-tBuC aggregates modulate their photochemistry.

Steady-state UV and FTIR spectroscopy show that hydrogen-bonded aggregates form by self-association of 4-tBuC molecules in cyclohexane solution. Electronic and vibrational transient absorption measurements are combined to identify and compare the photochemistry of isolated molecules to the aggregates. In agreement with Horbury et al. (25), the primary photochemical reaction of 4-tBuC in a weakly-interacting, nonpolar solvent is homolytic O-H bond dissociation, resulting in hydrogen atom ejection to the solvent and formation of a neutral semiquinone radical. In contrast, intermolecular hydrogen bonding in 4-tBuC aggregates fosters excited state structural relaxation and slows the O-H bond dissociation that ultimately gives rise to hydrogen-bonded neutral semiquinone radicals. Intermolecular hydrogen-bonding interactions and the associated changes in molecular conformation reveal potential mechanisms for photochemical modulation in hydrogen-bonded aggregates.

Materials and Methods

Sample preparation. For all solutions, 4-*t*-butylcatechol (4-tBuC) (Sigma Aldrich, >99.0%) was used as received and dissolved in cyclohexane (Acros, 99.99%). All measurements were performed on aerated solutions at room temperature.

Steady-state spectroscopy. UV-visible (UV-Vis) absorption spectra were collected using a Cary 5000 UV-Vis-NIR Spectrometer (Agilent; Santa Clara, CA). Solutions were measured in quartz cuvettes (for 0.5–10 mm path lengths) or CaF_2 demountable liquid cells (for 12–250 μm path lengths), depending on the concentration. For all spectra, the maximum absorbance was kept below 1.0.

Vibrational absorption spectra were collected using an FTIR spectrometer (FT/IR-4200, JASCO; Easton, MD). Samples were loaded into a custom-made demountable liquid cell with CaF_2 windows. Teflon spacers with various thicknesses (ranging 100–500 μm) were used depending on the solution concentration.

Transient absorption spectroscopy. Transient UV-Vis spectroscopy was performed using an ultrafast pump-probe spectrometer. The pump was generated by driving an optical parametric amplifier (TOPAS Prime, Coherent; Santa Clara, CA) tuned to 265 nm with the output of a ~100 fs Ti:Sapphire laser amplifier (Astrella, Coherent; Santa Clara, CA). The probe was a white light supercontinuum that was generated by focusing a portion of the Ti:Sapphire output onto a CaF_2 window. The excitation density at the sample position was ~900 μJ/cm^2 and ~413 μJ/cm^2 for 5 mM and 75 mM samples, respectively. The absorbed energy density was ~450 μJ/cm^2 and 370 μJ/cm^2 for the 5 mM and 75 mM samples, respectively. Solution samples were flowed during all measurements in a demountable CaF_2 flow cell (TFC-M25-3, Harrick Scientific Products; Pleasantville, NY), which was pumped using a peristaltic pump (Masterflex, Cole-Parmer; Vernon Hills, IL). The path lengths used were 500 μm and 100 μm for the 5 mM and 75 mM samples, respectively. Samples were replaced every ~10 minutes of scanning time in order to prevent measuring the build-up of *o*-quinone photoproducts. The transmitted probe beam was dispersed and detected using a prism spectrometer (2.0 VIS, Stresing Entwicklungsbüro; Berlin, Germany).

Time-resolved vibrational spectroscopy was performed using an ultrafast time-resolved infrared (TRIR) pump-probe spectrometer. The pump was generated by driving an optical parametric amplifier (OPerA Solo, Coherent; Santa Clara, CA) tuned to 265 nm with the output of a ~100 fs Ti:Sapphire laser amplifier (Libra HE, Coherent; Santa Clara, CA). The probe was generated by driving an optical parametric amplifier (TOPAS-C/nDFG, Coherent; Santa Clara, CA), which was tuned between 5.5 – 8 μm. The excitation density at the sample position was ~2 mJ/cm^2 and the absorbed energy density was ~1.6 mJ/cm^2. Solution samples were recirculated during all measurements through the same flow cell used for the transient UV-Vis measurements using a peristaltic pump (Masterflex L/S; Cole-Parmer, Vernon Hills, IL). The path lengths used were 500 μm and 100 μm for the 5 mM and 75 mM samples, respectively. Samples were replaced every ~10 minutes of scanning time in order to prevent measuring the build-up of *o*-quinone photoproducts. The transmitted probe beam was dispersed using a spectrograph (Triax, Horiba; Kisshoin, Japan) and

detected by a dual-row, 64-element/row, liquid N_2-cooled HgCdTe array (MCT-10-128, Infrared Associates; Stuart, Florida), and read out by a high speed integrator (FPAS-0144, Infrared Systems Development; Winter Park, FL).

UV-Irradiation experiments and in-situ absorption spectroscopy. UV irradiation experiments were performed using a homebuilt system. UV radiation from a deuterium lamp (Q Series, Newport; Irvine, California) was collected and focused onto the sample using parabolic reflectors. The beam was filtered using a 1 cm chloroform filter (cut-on was ~250 nm). *In-situ* absorption spectra were collected by measuring the transmitted light using a fiber-coupled CCD spectrometer (Flame-S, Ocean Optics; Largo, FL).

Quantum chemical computations. Calculations on the 4-tBuC monomer and dimer were carried out with density functional theory (DFT) and its time-dependent variant (TD-DFT) for the excited state. We calculated the ground- and excited-state structures and the excited state O-H dissociation paths. These paths were calculated as relaxed scans, freezing one internal coordinate to a fixed value and optimizing all of the remaining ones. We used the long-range corrected CAM-B3LYP functional, which avoids the appearance of spurious charge transfer excited states (26) and the 6-311G** basis set. These calculations were carried out with Gaussian 16 (27).

To support the identification of the neutral semiquinone radical we also calculated the vibrational frequencies of this species and its electronic spectrum. For the vibrational spectrum, we identified the most stable conformer and benchmarked the CAM-B3LYP/6-311G** level of theory with additional calculations on the phenoxyl radical. The electronic spectrum was calculated at the MS-CASPT2 level of theory (multi-state complete active space second order perturbation) with the ANO-L atomic natural orbitals basis set, using Molcas 7.8 (28). More computational details are in **Supporting Information** section **S.7**.

Results

UV absorption and FTIR spectra of 4-t-butylcatechol in cyclohexane

The UV-Vis absorption spectrum of a 6 mM solution of 4-tBuC in cyclohexane exhibits pronounced vibronic structure (**Figure 1a**), reminiscent of that of 4-tBuC in the gas-phase (25). As the concentration is increased above ~20 mM, the spectrum loses vibronic structure and blue shifts slightly. These high-concentration spectra resemble those of 4-tBuC in the hydrogen-bonding solvents water and acetonitrile (**Figure S1**).

FTIR spectra were recorded from catechol solutions with concentrations of 5 mM to 214 mM (**Figure 1b**). A dilute, 5 mM solution exhibits two narrow and intense absorption bands at 3576 cm^{-1} and 3624 cm^{-1}. As the concentration is increased to 38 mM, a broad absorption band appears at ~3440 cm^{-1}. Further increasing the concentration results in an even broader and more red-shifted absorption band at ~3400 cm^{-1}. Changes in the FTIR spectra are fully reversible, indicating that the spectral features are not indicative of chemical changes to the sample. The band assignments are listed in **Figure 1d** and possible hydrogen bonding patterns responsible for these frequencies are shown in **Figure 1e**. As in past work on cyclohexane solutions of phenol (29-32), a model was used to estimate the fraction of monomers and the fraction of dimers and higher-order aggregates (**Figure 1c**).

Transient UV-Vis spectroscopy of monomers and aggregates of 4-tBuC

UV-Vis transient absorption measurements were performed on 5 mM solutions (predominantly monomer-containing) and 75 mM solutions (primarily aggregate-containing, see discussion section) of 4-tBuC in cyclohexane with excitation at 265 nm (**Figure 2**). These concentrations represent the lowest and highest concentrations that are feasible for our instrumentation. The signals for the 5 mM solution agree very well with ones reported by Horbury et al. (25), while signals of 4-tBuC aggregates are reported here for the first time.

The transient absorption spectrum of the 5 mM sample at the earliest delay times spans our entire detection window from 320 to 650 nm and consists of several broad and overlapping peaks. During the first 50 ps, the signals decay to reveal strong photoinduced absorption (PIA) below 400 nm, which includes a very narrow absorption band at ~390 nm. An absorption onset appears below 340 nm. Across the entire measured spectral range, an additional PIA is observed (clearly evident in the 50 to 60 ps and 100 to 250 ps traces). This component matches the spectrum recorded from cyclohexane under identical measurement conditions (black curve in **Figure 2a**). There is an additional weak, but detectable, absorption band occurring around 600 nm (see 2000-3000 ps trace in **Figure 2a**) that is distinct from the spectrum measured from neat cyclohexane.

The 75 mM sample also exhibits a prompt, broad PIA feature, which spans the entire measured spectral region and is very similar to the spectrum recorded at the same delay time for the 5 mM solution (**Figure 2b**). This feature decays more slowly than in the 5 mM sample on the early picosecond timescale. At the longest time delays (i.e., 2000 to 3000 ps), a broad PIA band is observed in the 320 to 400 nm spectral range that differs in several respects from the band seen in

the 5 mM solution. In particular, the narrow peak centered at 390 nm in the 5 mM solution is not observed in the 75 mM solution. A maximum is also seen in the 75 mM solution near 350 nm, while the signal in the 5 mM solution rises monotonically below 380 nm. Unlike the 5 mM solution, the 75 mM solution exhibits a transient band near 625 nm, which is readily seen between 50 and 250 ps (**Figure 2b**).

Kinetic traces for the 5 mM and 75 mM samples are compared in **Figure 3**. The traces were generated by averaging the signals over the indicated wavelength ranges. Three key features in the kinetics of the 5 mM sample are observed. First, there is a fast decaying component present for all three wavelength ranges shown, which is primarily associated with the PIA feature spanning 320 to 660 nm. Second, the signal in the 350 to 370 nm trace persists beyond the longest recorded delay time of ~3 ns. Third, an additional slowly decaying component can be seen at times greater than ~40 ps in the 480 to 500 nm and 600 to 650 nm traces. Matching decay kinetics are seen over the same time interval when exciting neat cyclohexane under identical experimental conditions (gray curve in **Figure 3a**).

The kinetic traces from the 75 mM sample differ in several important aspects from the ones measured for the 5 mM solution. First, the PIA feature spanning 320 to 660 nm decays more slowly in the more concentrated solution as seen by comparing the 480 to 500 nm traces in **Figure 3**. Second, an additional kinetic component that decays on a hundreds of picoseconds timescale is seen in the 600 to 650 nm trace of the 75 mM solution, but not in the 5 mM sample. This decay component is likely associated with the band centered at ~625 nm that is observed in the 75 mM solution but absent in the 5 mM solution. Last, the signal arising from excitation of the solvent contributes marginally to the observed kinetics for the 75 mM sample because a much smaller path length was used. It is also important to note that the neat solvent signal represents an upper limit to the signal contribution in solutions where the solute absorbs a large fraction of the pump pulse. Similar to the 5 mM sample, there is a persistent signal observable in the 350–370 nm trace.

Time-resolved vibrational spectroscopy of monomers and aggregates of 4-*t*-butylcatechol

For time-resolved infrared (TRIR) measurements, the minimum concentration that could be studied was 10 mM, and not 5 mM, due to the detection limit of our TRIR spectrometer. It should

also be noted that a broad positive absorption signal arising from solvent excitation was removed from the data by subtraction as described in the **Supporting Information** (section **S.3**). The results are shown in **Figure 4** for both 10 mM (primarily monomer) and 75 mM (primarily aggregate) solutions of 4-tBuC in cyclohexane.

Immediately after photoexcitation, the 10 mM sample exhibits ground state bleaches (GSBs) at 1290 cm^{-1}, 1508 cm^{-1}, 1527 cm^{-1}, and 1610 cm^{-1}, and PIAs at 1341 cm^{-1}, 1406 cm^{-1}, <1485 cm^{-1}, 1552 cm^{-1}, and 1575 cm^{-1}. The PIA bands decay on a time scale similar to that of the $S_1 \rightarrow S_n$ absorption feature measured using transient UV-Vis spectroscopy. As these PIA bands decay, a pair of positive bands grow in at 1632 cm^{-1} and 1662 cm^{-1}. Additional weaker PIA bands are observed at 1552 cm^{-1} and 1587 cm^{-1}. These four PIA bands persist out to the nanosecond timescale.

The 75 mM sample exhibits a similar set of negative and positive absorption bands immediately following 265 nm photoexcitation, including GSBs at 1289 cm^{-1}, 1509 cm^{-1}, 1526 cm^{-1}, and 1609 cm^{-1}, and PIAs at 1339 cm^{-1}, 1406 cm^{-1}, 1481 cm^{-1}, 1548 cm^{-1}, and 1582 cm^{-1}. These PIA features decay over tens of picoseconds, or somewhat more slowly than those in the 10 mM sample. An intense, broad PIA band grows in around 1645 cm^{-1}. Additional broad PIA bands are revealed at <1467 cm^{-1} and ~1566 cm^{-1}. These PIA bands persist into the nanosecond timescale. Notably, the 1566 cm^{-1} and 1645 cm^{-1} bands observed in the 75 mM sample are located at approximately the mean position of the corresponding bands observed in the 10 mM sample, between the 1587 cm^{-1} and 1552 cm^{-1} bands, and the 1632 cm^{-1} and 1662 cm^{-1} bands, respectively.

Kinetic analysis of the time-resolved vibrational spectra provides further insight into the population dynamics. The kinetics corresponding to three of the most dominant features in the transient absorption spectra are shown in **Figure 5**. The traces in the figure were obtained by averaging over the spectral ranges indicated by boxes of the same color in **Figure 4**. For both solute concentrations, the kinetics for the absorbing species that appears immediately upon photoexcitation is isolated by averaging the ~1341 cm^{-1} and 1406 cm^{-1} PIA bands to improve signal-to-noise (S/N) (red curves in **Figure 5**). The kinetics for the positive absorbing species at later time delays is obtained from the band present around 1650 cm^{-1} (blue curves). The recovery of the ground state population for both samples was followed using the GSB peak at ~1290 cm^{-1}, which is devoid of spectral contamination by PIA features.

For the 10 mM sample, the PIA decays biexponentially with a fast ~12 ps decay component and a slow ~180 ps decay component. The PIA signal at ~1650 cm^{-1} (blue curve) also exhibits biphasic behavior, quantitatively mirroring the two components of the GSB decay kinetics. The GSB signal (black squares, **Figure 5c**) does not decay within the entire time window.

For the 75 mM sample, the PIA bands decay more slowly over the first 100 ps than is the case for the 10 mM sample. The kinetics resemble the $S_1 \rightarrow S_n$ PIA decay kinetics for the 75 mM solution measured using transient UV-Vis spectroscopy (green and red curves in **Figure 3b**). The growth kinetics of the 75 mM sample (blue curve in **Figure 5b**) also exhibits complex behavior, and the growth at early time delays does not match the decay of the PIA signal (red curve in **Figure 5b**) at early time delays. Unlike for the case of the 10 mM solution, the GSB signal of the 75 mM solution decreases in absolute value over the 10s to 100s of picoseconds timescale, indicating partial recovery of the ground state population. This GSB decay trace (gray squares, **Figure 5c**) resembles the decay of the PIA feature (red trace in **Figure 5b**).

UV-irradiation of 4-*t*-butylcatechol solutions

Absorption spectra recorded from samples exposed to continuous UV irradiation from a filtered deuterium lamp for up to 30 minutes are shown in **Figure 6** for the 5 mM and 75 mM 4-tBuC solutions. In both solutions, the absorption band at ~281 nm decreases and a broad absorption band appears between 350 and 450 nm with increasing irradiation time, demonstrating that photoproducts accumulate in significant quantities after several minutes of UV irradiation.

O-H dissociation and H-atom transfer calculations

Density functional calculations (CAM-B3LYP functional, see **Materials and Methods**) were performed on the 4-tBuC monomer and dimer to gain insight into the reaction pathways (**Figure 7**). Exploratory calculations showed that there are several dimer conformations with different H-bonding patterns within a narrow energy range, but in every structure each of the OH groups participates in an intermolecular hydrogen bond. Here we focus on the structure displayed in **Figure 7b**, which is also representative of calculated trimers with similar H-bonding patterns. It has three intermolecular H-bonds, two weakened intramolecular H-bonds compared to the monomer (O-H distances increase from 2.11 to 2.37-2.38 Å), and a free O-H group. The calculations suggest that the excitation is localized on a single catechol molecule. Upon relaxation on S_1, there are significant changes in the intermolecular H-bonds, and one of these bonds stretches from 2.01 to 3.12 Å.

In our calculations, we estimated the energetics of the excited-state dissociation of the free O-H bonds of the monomer and dimer and, as an alternative pathway, photoinduced H-atom transfer along hydrogen bonds. The latter reaction was considered both for H-atom transfer along the intramolecular hydrogen bond in the monomer as well as along the intermolecular hydrogen bond joining two catechol units in the dimer. The calculated activation energy barriers for these pathways, which correspond to weakly avoided crossings between the S_1 and S_2 adiabatic states (33), are collected in **Table 1**, and the potential energy profiles are described in the Supporting Information (**Section S.7**).

The dissociation reactions of free O-H groups in the monomer and dimer have almost equal activation energy barriers. This suggests that any tunneling contribution to the O-H dissociation (33) will be similar for the two species. In contrast, the activation energy barriers for photoinduced transfer of an H atom along a hydrogen bond, whether this occurs intramolecularly in a single 4-tBuC molecule or between two 4-tBuC molecules connected by an intermolecular hydrogen bond, are ~5-7 times higher compared to the dissociation of a free O-H bond.

Discussion

Self-association and intermolecular hydrogen bonding in 4-*t*-butylcatechol solutions

At low concentrations, 4-tBuC does not hydrogen bond significantly with itself and a gas-phase-like UV absorption spectrum with sharp vibronic structure is observed (**Figure 1a**). As previously observed for phenol (29-32), 4-tBuC forms aggregates at high solute concentrations in cyclohexane. Aggregates form when the total concentration of 4-tBuC exceeds approximately 5 mM, according to analysis of the electronic and vibrational absorption spectra in **Figure 1a** and **1b**. The loss of vibronic structure with increasing 4-tBuC concentration reflects intermolecular hydrogen bonding between 4-tBuC molecules.

FTIR spectroscopy provides a direct means of assessing intramolecular and intermolecular hydrogen bonding through changes in O-H absorption lineshapes. The FTIR spectrum of the 5 mM solution (**Figure 1b**) features two narrow and intense absorption bands at 3576 cm^{-1} and 3624 cm^{-1}, which are assigned to the intramolecularly hydrogen-bonded (“b”) and free (“f”) O-H local stretching modes (**Figure 1e**), respectively, based on catechol studies (34-36). CAM-B3LYP calculations on the monomer support this assignment, giving frequencies of 3826 cm^{-1} and 3892 cm^{-1} for the "b" and "f" modes. These values are in good agreement with experiment when a scaling factor of 0.93 is applied. Note that our use of the term, “free O-H”, signifies that the O-H group does not donate a hydrogen bond, although it may still accept a hydrogen bond as this does not lead to a frequency

shift of the O-H stretch as seen in other hydrogen-bonded alcohols such as methanol (37). The observation of intramolecular hydrogen bonding of 4-tBuC supports the work of Horbury et al. (25), which deduced that the molecules primarily assume an intramolecularly hydrogen-bonded ("closed") form in cyclohexane. As the concentration is increased much broader lower-frequency bands appears with maxima around 3440 cm^{-1} and 3400 cm^{-1}, indicating the formation of intermolecularly hydrogen-bonded aggregates (29).

Both the f and b bands appear to disappear in unison as the concentration of 4-tBuC is increased. This differs from the behavior observed when a base such as diethyl ether is added to catechol in carbon tetrachloride where the intensity of the free O-H stretching band is diminished before a decrease is observed in the intramolecularly hydrogen-bonded band (38). This is because the base initially hydrogen bonds to the free O-H group, and the intramolecular hydrogen bond remains intact. A similar phenomenon was observed when adding DMSO to 3,5-di-*t*-butylcatechol in carbon tetrachloride (39).

The difference in behavior may be because the addition of a 4-tBuC monomer to another monomer or aggregate not only causes the loss of a free OH bond, but also simultaneously perturbs the intramolecular hydrogen bond. The calculated dimer structure shown in **Figure 7** shows how this might happen. In this structure, one O-H group on each molecule forms a bifurcated hydrogen bond: The intramolecular hydrogen bond weakens and becomes longer, but the same hydrogen participates in a second, stronger intermolecular hydrogen bond (see also the bifurcated aggregate structure in **Figure 1e**). The latter effect is expected to redshift the frequency of the O-H group that formerly participated only in intramolecular hydrogen bonding. Consistent with this idea, CAM-B3LYP calculations for the dimer shown in **Figure 7b** give stretching frequencies for the two bifurcated O-H groups of 3412 cm^{-1} and 3468 cm^{-1}, applying the correction factor of 0.93 suggested by the calculations for the monomer.

The self-association of 4-tBuC in cyclohexane leads to spectral changes in the O-H stretching region of the FTIR spectrum (**Figure 1b**) that closely resemble changes arising from the aggregation of phenol in cyclohexane (29, 31). Extensive modeling of cyclohexane solutions of phenol has revealed a complex equilibrium between monomers, dimers, and multimers (29-32). Adapting from these models, the fractions of monomers and aggregates containing at least two 4-tBuC molecules were determined (**Figure 1c**). Further details are provided in the **Supporting Information** (section **S.3**).

UV-irradiation of 4-*t*-butylcatechol solutions

The photoproducts of UV-irradiated 4-tBuC were identified using time-dependent UV-Vis spectroscopy (see **Figure 6**) in order to assist interpretation of the time-resolved spectroscopy results. The **Supporting Information** includes an expanded analysis of the time-dependent absorption spectra and further details about the experimental design. In both the 5 mM and 75 mM samples, new red-shifted absorption bands appear over time. These bands are assigned to *o*-quinones, the fully oxidized form of catechol (40-42). This assignment is supported by mass spectrometry measurements made with the 5 mM sample (**Figure S9**). Note that the quinone bands in the 5 mM and 75 mM samples are centered at 370 nm, and 400 nm, respectively. The redshift and broadening of this band is attributed to hydrogen bonding between the quinone and catechol species (see **Figure S7**). The quantum yields of quinone formation were determined to be 2.5% and 0.4% for the 5 mM and 75 mM solutions, respectively (see the **Supporting Information** for details). Despite the differences in transient absorption signals observed for 4-tBuC monomers and aggregates in cyclohexane, photoexcitation of each leads to similar photoproducts, albeit with a lower quantum yield for the 75 mM solution.

Photochemistry of 4-*t*-butylcatechol monomers

We first discuss the time-resolved spectroscopy of the 4-tBuC monomer because its electronic spectroscopy aids analysis of the photochemical dynamics of the aggregates, which are presented here for the first time. The solutions were excited at 265 nm, a wavelength known to directly populate the S_1 state, which has $^1\pi\pi^*$ character at the Franck-Condon geometry (25). The PIA feature appearing at 1–2 ps in the 5 mM sample (red trace in **Figure 2a**) was previously assigned by Horbury et al. (25) to $S_1 \rightarrow S_n$ absorption by 4-tBuC. This PIA spectrum evolves into a feature below 400 nm possessing a sharp peak at ~390 nm, which Horbury et al. (25) assigned to a neutral 4-tBuC semiquinone radical (structure shown in **Scheme 1**). This feature resembles the sharp band observed at 383 nm in the absorption spectrum of the neutral semiquinone radical of catechol in liquid paraffin (43). A weak feature around 600 nm is also expected for the semiquinone radical based on the absorption spectrum of the phenoxyl radical (44). MS-CASPT2 calculations predict absorption peaks at 349 nm and 583 nm for the 4-tBuC semiquinone radical (see **Table S3**), supporting our assignment. The additional absorption onset appearing below 340 nm is tentatively assigned to a further photoproduct (see below).

The UV photochemistry of 4-tBuC monomers in cyclohexane mirrors that of catechol (33, 45) and phenol (46, 47). Excitation to the S_1 state, which has $^1\pi\pi^*$ character initially, causes O-H dissociation via tunneling to the dissociative $^1\pi\sigma^*$ state (33). This occurs at a weakly avoided crossing where S_1 changes from $^1\pi\pi^*$ to $^1\pi\sigma^*$ character. Horbury et al. (25) observed that photoinduced O-H bond dissociation of 4-tBuC upon 267 nm excitation occurs with a time constant of 18 $\pm$ 1 ps in cyclohexane and 4.9 $\pm$ 0.6 ps in the gas phase. A somewhat shorter time constant of 12.15 ± 0.03 ps was observed in our study for 4-tBuC in cyclohexane solution following 265 nm excitation (see **Figure 2** and **Supporting Information** for a detailed target analysis). The slower dissociation time in ref. (25) could be due to the seven-fold higher solute concentration compared to ours (35 mM vs. 5 mM). According to our analysis of the data in **Figure 1**, a concentration of 35 mM is high enough to have a significant population of aggregates, which result in more slowly decaying signals (see below).

Despite using moderate excitation conditions (i.e., ~900 μJ/cm^2), the long path length of 500 μm needed to obtain an appreciable UV optical density for the 5 mM sample increases the signal contribution from solvent ionization (48). This produces a PIA feature spanning the entire spectral range measured for the 5 mM sample, which is identified in a neat cyclohexane solution measured under identical conditions (black trace in **Figure 2a**). The solvent-only signal is successfully accounted for in the target analysis model used to obtain the time constant for O-H dissociation in the 5 mM solution (see **Figure S14** for further details). Because of this, and because its signal strength contributed only modestly to the total observed sample signal, we did not subtract it prior to kinetic analysis.

The TRIR spectrum of the 4-tBuC monomer in cyclohexane exhibits several prompt PIA features (see the red trace in **Figure 4a**) that decay with a time constant of ~12 ps, a value that matches the lifetime of the $S_1 \rightarrow S_n$ feature determined from transient UV-Vis spectroscopy. As such, we assign these vibrational features to the S_1 electronic state. Note that this S_1 vibrational spectrum of 4-tBuC resembles that reported for phenol in cyclohexane (46). The occurrence of these intense, low-frequency PIA bands (relative to the C=C ring stretching GSB bands) is reflective of a break in ring planarity (49, 25, 50) of the S_1 state of 4-tBuC.

As the PIA bands of the S_1 state decay, new PIA features appear around 1662 cm^{-1}, 1587 cm^{-1}, and 1552 cm^{-1}. The most prominent band at ~1650 cm^{-1} has an initial formation time constant of ~12 ps, which matches the decay time of the S_1 absorption bands observed in the TRIR spectrum, and the O-H dissociation time constant determined using transient UV-Vis spectroscopy. Combining

the vibrational and electronic data, we assign the features at 1662 cm^{-1}, 1587 cm^{-1}, and 1552 cm^{-1} to neutral semiquinone radicals of 4-tBuC, formed from O-H bond dissociation. Our DFT calculations (see **Supporting Information**, Section **S7**) support this assignment. The formation kinetics of the ~1662 cm^{-1} band exhibits biexponential growth, with a slower component occurring on the tens to hundreds of picosecond timescale in addition to the fast ~12 ps component.

There are three possible explanations for this kinetic behavior. First, we considered that hot ground electronic states might produce the slowly decaying positive feature observed near 1650 cm^{-1}. However, the GSB kinetics at 1290 cm^{-1} in the 10 mM solution (see **Figure 5c**) exhibit practically no change in intensity across the entire time window, indicating that the depleted ground state population remains constant and is not restored via internal conversion. Additionally, temperature-dependent FTIR experiments (see **Figure S17**) show that the probed C=C ring stretching mode at ~1610 cm^{-1} is insensitive to temperature change and cannot explain the positive feature at ~1650 cm^{-1}.

Second, we considered the possibility that aggregates contribute to the spectrum because approximately 25% of the 4-tBuC molecules in the 10 mM sample are present as dimers or higher aggregates. The S_1 PIA decay kinetics and the 1662 cm^{-1} growth kinetics are biexponential, with weighting factors of 0.75 and 0.25 for the fast and slow components, respectively. The relative amplitude of the fast and slow component is in excellent agreement with the fraction of monomer (75%) and aggregates (25%) present in 10 mM solution, based on our self-association modeling (see **Figure 1**). The fast component decays with a time constant of ~12 ps in agreement with the lifetime of the 4-tBuC monomer observed in the transient UV-Vis experiment. The longer-lived component decays on a similar timescale as the excited singlet state in the aggregates (see 75 mM data in **Figure 2** and **Figure 3**). This evidence thus suggests that there is a small population of longer-lived excited states of aggregates present in the 10 mM solution that contributes to the total TRIR spectrum. In this case, the slow growth of the 1662 cm^{-1} band is assigned to UV-excitation of 4-tBuC aggregates.

Third, it was considered that some of the ejected H-atoms might recombine geminately with semiquinone radicals, producing cyclohexadienone photoproducts like the ones shown in **Scheme 1**. If these adducts possess vibrational spectra similar to that of the semiquinone radical, then the slower growth at 1650 cm^{-1} could simply reflect the time scale of geminate recombination, which commonly occurs on the tens to hundreds of picoseconds timescale (51-54). For example, the formation of cyclohexadienone via recombination is observed after photodissociation of phenol in

cyclohexane. Harris et al. (46) assigned a feature at 1671 cm^{-1} in an 8 mM solution of phenol dissolved in cyclohexane to either a cyclohexa-2,4-dienone or a cyclohexa-2,5-dienone. Isolation of unsubstituted cyclohexadienones for spectroscopic study is very difficult due to their instability (55, 56). Nonetheless, prior experimental and computational reports (55, 57) suggest that they contain intense vibrational peaks around 1670 cm^{-1} and 1636 cm^{-1}, corresponding to C=O and C=C stretching modes (57). In addition, the FTIR spectrum of a brominated cyclohexa-2,5-dienone derivative (**Figure S18**) has a pair of peaks that resembles the 1000 to 3000 ps TRIR spectrum of the 10 mM sample, although they appear at somewhat higher frequencies (1675 cm^{-1} and 1685 cm^{-1}) likely due to different aromatic substituents.

In the transient UV-Vis spectrum, the absorption onset below 340 nm for the 5 mM solution (**Figure 2a**) is not seen in the neutral semiquinone radical (43). Instead, this absorption onset qualitatively matches that of the brominated cyclohexa-2,5-dienone derivative (see **Figure S18**). Previous pulse radiolysis studies of OH adducts of phenol (58), catechol (59), and 4-tBuC (60) reveal that their hydroxycyclohexadienyl radicals, which are similar in chemical structure to cyclohexadienones, possess absorption spectra similar to those of cyclohexa-2,4-dienone (61) and cyclohexa-2,5-dienone (62) derivatives. The absorption spectrum of each of these compounds also qualitatively matches the absorption below 340 nm in monomers of 4-tBuC. However, while cyclohexadienone formation explains the second growth component seen for the ~1662 cm^{-1} PIA feature, it cannot explain the slow decay of the S_1 PIA features at ~1341 cm^{-1} and ~1406 cm^{-1} (red trace in **Figure 5a**). We therefore favor the second explanation above in which a minor amount of aggregates results in a slowly forming population of semiquinone radicals. Regardless of whether dimers or cyclohexadienones contribute to the PIA band at ~1650 cm^{-1}, all of the PIA bands in the 1000 to 3000 ps trace in **Figure 4a**, including the ~1650 cm^{-1} feature, must be at least partially attributable to neutral semiquinone radicals of 4-tBuC.

Photochemistry of 4-*t*-butylcatechol hydrogen-bonded aggregates

Transient absorption by the initially photogenerated state in the 75 mM solution resembles that observed in the 5 mM solution (compare 1 – 2 ps spectra in **Figure 2**). Based on these similarities and our TD-DFT results, we propose that the initially photogenerated S_1 state in aggregates is a locally excited singlet state, which is minimally perturbed by neighboring molecules. This PIA feature decays more slowly in the aggregates, evolving on the tens of picoseconds timescale into a red-shifted spectrum with the longest wavelength peak appearing beyond 600 nm. This indicates structural relaxation of the excited state. At later times, the spectrum features a peak

around 355 nm that persists for nanoseconds. This feature resembles that observed for the neutral semiquinone radical in the 5 mM sample, but lacks the sharp band at ~390 nm. The appearance of semiquinone radicals indicates that O-H dissociation also occurs in aggregates. The assignments of these features will be discussed later.

The first obvious difference in the transient spectra is that the S_1 feature decays more slowly in the 75 mM solution compared to the 5 mM solution, with a fast time constant of at least ~24 ps and a slow time constant of at least ~154 ps (depending on the target model used; see **Figures S15** and **S16**). Excited state relaxation in aggregates occurs more slowly than O-H dissociation in monomers, suggesting that differences in the aggregate excited state potential energy landscape hinder this reaction. However, the lifetime of the S_1 feature (~154 ps, see **Figures S15**) in the 75 mM solution is still much shorter than the lifetime of 1.7 ns measured by Horbury et al. for 265 nm excitation of 4-tBuC dissolved in acetonitrile (25), indicating that nonradiative decay proceeds at a higher rate in the hydrogen-bonded aggregates.

The second obvious difference in the spectral dynamics for the 75 mM solution is that the initial PIA feature evolves on the tens of picoseconds timescale, revealing a low-energy peak at ~625 nm (see 50 to 60 ps spectrum in **Figure 2b**). We assign this new spectrum to locally excited S_1 states that have undergone structural relaxation, leading to a change in electronic density in the ring system, based on the following considerations. First, this spectrum resembles that of the initially photogenerated S_1 state absorption. Second, its spectral shape is highly reminiscent of the S_1 absorption spectrum of dilute solutions of phenol in cyclohexane excited at 265 nm (47) or 267 nm (46). Phenol contains one fewer hydroxy group (**Scheme 1**), suggesting that there is less electronic density on the ring than in 4-tBuC. Third, the S_1 state of guaiacol in cyclohexane has been shown to have an absorption peak beyond 600 nm (63). Guaiacol contains an *ortho*-positioned hydroxy and methoxy group (**Scheme 1**), suggesting that the aromatic ring may possess an electron density inbetween that of phenol and 4-tBuC. Altogether, we propose that the locally excited S_1 states in 4-tBuC aggregates relax because of structural rearrangements within the hydrogen-bonded aggregates, changing the $S_1 \rightarrow S_n$ spectrum. Consistent with our spectroscopic assignment, the calculated changes in O-H hydrogen bond distances between the ground and excited states of 4-tBuC dimers (**Figure 7b**) indicate that the aggregates may undergo significant conformational rearrangements after excitation.

Note that phenol excimers have been reported to absorb in the visible spectral region (47), however we do not observe a clear signature of excimers in 4-tBuC aggregates. This difference in behavior can be rationalized by considering the much longer S_1 lifetime (i.e., 2.1 ns) of the phenol monomer, and the even longer lifetime of the phenol excimer (47). In 4-tBuC, excimer formation is unlikely to compete kinetically with the decay of S_1, which has a lifetime approximately one order of magnitude shorter than in analogous phenol aggregates. Furthermore, substantial rearrangements of the molecules are expected in order to transition from the predicted ground state geometry (e.g., the dimer structure in **Figure 7b**) to the expected excimer geometry, which in the case of phenol involves a pseudo-parallel π-stacked geometry (64).

The TRIR spectrum of the 75 mM solution (see **Figure 4**) closely resembles that of the 10 mM solution, but the decay and growth of the vibrational features are slower. In particular, the vibrational spectrum measured 1 ps after photoexcitation contains the same PIA bands seen in the 10 mM sample, which are assigned to the S_1 electronic state. These bands decay on the tens-to-hundreds of picoseconds timescale, without significant changes in lineshape. Excimers and exciplexes have been shown in the past to produce TRIR spectra with frequencies and lineshapes that are readily distinguishable from those of locally excited or ionic states (65-67). In particular, the broadened distribution of nuclear geometries that accompanies excimer or exciplex formation yields significantly broadened vibrational spectra (67, 65, 66). Because the vibrational bands do not exhibit any peak shifting or broadening during the timescale in which the excited electronic state relaxes (several tens of picoseconds), it is unlikely that excimers are formed. Instead, it is more likely that the excited singlets of the 4-tBuC aggregates remain as locally excited states during structural relaxation.

The TRIR spectra of the 75 mM sample at later delay times resemble the 1000 to 3000 ps spectrum of the 10 mM sample, except with significantly broadened absorption peaks at approximately 1566 cm^{-1} and 1645 cm^{-1}. The similar vibrational frequencies of the bands observed for both the 10 mM and 75 mM samples suggest common transient species, namely, semiquinone radicals of 4-tBuC. Furthermore, both monomer and aggregate solutions produce *o*-quinones in the UV-irradiation experiments, suggesting that the semiquinone radical is a common reaction intermediate. The broadening of the semiquinone vibrational spectrum is proposed to be a consequence of aggregation, where the radical species experience intermolecular hydrogen bonding like ground state molecules. Note that an analogous vibrational peak-broadening phenomenon has also been reported for exciplexes in solution (66).

As indicated in **Figure 1c**, the 75 mM solution contains ~25% monomers and so it is reasonable to believe that the semiquinones may form exclusively from monomers. It is difficult to discern the monomer contribution to the transient UV-Vis spectra (**Figure 2** and **3**) both visually and using target analysis due to multiple overlapping features. However, the TRIR kinetics of the semiquinone band at ~1645 cm^{-1} (blue trace in **Figure 5b**) clearly show a continuous growth of its population over the entire time window. Such behavior cannot be explained by monomers, which yield a single lifetime of ~12 ps.

Transient absorption spectroscopy clearly reveals that O-H dissociation is slower in 4-tBuC aggregates than in monomers. While the FTIR results suggest that the aggregates are composed of extended hydrogen-bonded networks of 4-tBuC molecules that exhibit hydrogen bonds to both O-H groups, it is instructional to consider a 4-tBuC dimer. Our TD-DFT calculations on the dimer predict a ~5-fold increase in activation energy barrier for H-atom transfer compared to the dissociation of a free O-H bond. Poterya et al. considered analogous pathways in their computational study of hydrogen-bonded clusters of phenol in the gas phase (68). Their calculations predict a larger barrier for the H-atom transfer pathway (1.0 eV) than for the dissociation of a free H-bond (0.9 eV), although the difference in barriers is much less pronounced than in our calculations for 4-tBuC. In fact, the barrier height of 0.51 eV (Table 1) calculated for H-atom transfer along an intermolecular H bond is too large to explain the appearance of the semiquinone radical in our measurements in no more than several hundred ps. Of course, tunneling under the barrier could take place, but further study is warranted of how hydrogen bonding in 4-tBuC aggregates retards OH bond dissociation.

Our observations are consistent with a previous study of phenol dimers, which attributed the observed increase of the S_1 lifetime to a decrease in O-H dissociation efficiency compared to monomers (47). The authors considered that hydrogen bonding between phenol molecules may cause the repulsive S_2 state ($^1\pi\sigma^*$) to become bound at larger O-H bond distances (47), based on calculations of the excited state of dimeric water (69). Our experimental and computational evidence for S_1 structural relaxation, in addition to the measured partial GSB recovery, in 4-tBuC aggregates suggests that intermolecular hydrogen bonding hinders O-H dissociation by a similar mechanism. Nevertheless, O-H dissociation still takes place in 4-tBuC aggregates, and further study is warranted to determine whether dynamic fluctuations of the hydrogen bonds or other factors regulate this process.

We tested two possible kinetic models for describing excited state processes in 4-tBuC aggregates using target analysis (see **Figure S15–16**). In the sequential decay scheme, the S_1 states undergo structural relaxation preceding O-H dissociation. In the parallel decay scheme, O-H dissociation occurs only from S_1 states that have not had time to structurally relax. While both schemes fit the data equally well, we propose that only the sequential pathway shown in **Scheme 2** is adequate. According to this model, structural relaxation of the S_1 state occurs with a time constant of 23.6 ± 0.2 ps, and is followed by competitive deactivation via internal conversion (154 ± 2 ps) or O-H bond dissociation (190 ± 20 ps). Using these time constants, 55% of the excited population is predicted to decay by internal conversion in excellent agreement with the loss of 57% of the initial bleach amplitude seen in the TRIR GSB signal in **Figure 5c**. On the other hand, the parallel model is less satisfactory as it predicts that 81% of the population decays by internal conversion.

Examination of the excited state decay times of 4-tBuC monomers and aggregates provides further insights. Horbury et al. (25) proposed that because the ground electronic state of 4-tBuC is planar, the break in ring planarity of the S_1 state of 4-tBuC results in symmetry-enhanced tunneling that promotes O-H bond dissociation. This phenomenon is favored in cyclohexane, in which 4-tBuC exists predominantly in an intramolecularly hydrogen-bonded (or "closed") geometry (25). In contrast, 4-tBuC exists predominantly in a non-intramolecularly hydrogen-bonded (or "open") geometry in polar solvents like acetonitrile, resulting in a planar S_1 state that is unlikely to undergo O-H dissociation (25).

Our FTIR results support their work by providing direct evidence for intramolecular hydrogen bonding in 4-tBuC monomers in cyclohexane. Our transient UV-Vis data demonstrate that 4-tBuC aggregates in cyclohexane possess a longer S_1 lifetime than monomers, by at least an order of magnitude. Variations in the O-H stretch lineshape with concentration (**Figure 1b** and **1c**) suggest that molecules in aggregates exist in a slightly less "closed" form in the ground state than monomers. Additionally, the changes in hydrogen bond distances predicted by 4-tBuC dimer computations (see **Figure 7**) suggest that intramolecular hydrogen bonds are weakened in aggregates. This change in ground state conformation relative to the monomer leads to the prediction of a more planar S_1 state, which could further inhibit O-H dissociation due to closer symmetry to the S_0 state. These observations form an additional potential mechanism for inhibiting O-H bond dissociation and allowing internal conversion to proceed in aggregates (recall the observation of partial ground state recovery in **Figure 5c**).

Conclusion and Outlook

To date, most spectroscopic work has investigated the photochemistry and photophysics of monomeric models of eumelanins (22, 25, 19) and small oligomer and polymer models (20, 21), in addition to eumelanin itself (23, 70). Additionally, solvent-mediated excited state deactivation has been studied (20). While the participation of solvent on the excited state dynamics following photoexcitation of these model systems is generally understood, less attention has been paid to understanding how direct intermolecular interactions between eumelanin units affect excited state relaxation. Past studies have emphasized that covalent dimerization and oligomerization of eumelanin building blocks is important for shortening their excited state lifetimes in aqueous solution (20, 21). However, our results show that turning on intermolecular interactions from monomer to aggregates of 4-tBuC elongates its excited state lifetime. Because dihydroxy functionalized subunits in the eumelanin polymer may be located within domains that are hardly influenced by the solvent, alternative excited state deactivation pathways and their photochemical consequences should be considered.

Acknowledgements

CG thanks Joshua Snyder and Jacob Remington for helpful discussions and Andrew Pinkham for assistance with the mass spectrometry measurements. BK acknowledges funding from The Ohio State University. LB acknowledges financial support from the Spanish Ministerio de Economía y Competitividad (CTQ2015-69363-P) and computational time from Consorci de Serveis Universitaris de Catalunya.

Supporting Information

Supporting Information can be found in the online version of this article, which includes additional UV-Vis and FTIR absorption spectra and analysis, further information on the transient absorption measurements and target analysis, mass spectrometry results, quinone quantum yield calculations, and related computational results.

References

1. d'Ischia, M., A. Napolitano, A. Pezzella, P. Meredith and T. Sarna (2009) Chemical and structural diversity in eumelanins: Unexplored bio-optoelectronic materials. *Angew. Chemie* **48,** 3914-3921.
2. Dreyer, D. R., D. J. Miller, B. D. Freeman, D. R. Paul and C. W. Bielawski (2012) Elucidating the structure of poly(dopamine). *Langmuir* **28,** 6428-6435.
3. Głowacki, E. D., M. Irimia-Vladu, S. Bauer and N. S. Sariciftci (2013) Hydrogen-bonds in molecular solids – from biological systems to organic electronics. *J. Mat. Chem. B* **1,** 3742.
4. Liu, Y., K. Ai and L. Lu (2014) Polydopamine and its derivative materials: Synthesis and promising applications in energy, environmental, and biomedical fields. *Chem. Rev.* **114,** 5057-5115.
5. Zedler, L., M. D. Hager, U. S. Schubert, M. J. Harrington, M. Schmitt, J. Popp and B. Dietzek (2014) Monitoring the chemistry of self-healing by vibrational spectroscopy – current state and perspectives. *Mater. Today* **17,** 57-69.
6. Faure, E., C. Falentin-Daudré, C. Jérôme, J. Lyskawa, D. Fournier, P. Woisel and C. Detrembleur (2013) Catechols as versatile platforms in polymer chemistry. *Prog. Polym. Sci.* **38,** 236-270.
7. Filippidi, E., T. R. Cristiani, C. D. Eisenbach, J. H. Waite, J. N. Israelachvili, B. K. Ahn and M. T. Valentine (2017) Toughening elastomers using mussel-inspired iron-catechol complexes. *Science* **358,** 502-505.
8. Wu, J., L. Zhang, Y. Wang, Y. Long, H. Gao, X. Zhang, N. Zhao, Y. Cai and J. Xu (2011) Mussel-inspired chemistry for robust and surface-modifiable multilayer films. *Langmuir* **27,** 13684-13691.
9. Nicolas, J. J., F. C. Richard-Forget, P. M. Goupy, M. J. Amiot and S. Y. Aubert (1994) Enzymatic browning reactions in apple and apple products. *Critical reviews in food science and nutrition* **34,** 109-157.
10. Holderbaum, D. F., T. Kon, T. Kudo and M. P. Guerra (2010) Enzymatic browning, polyphenol oxidase activity, and polyphenols in four apple cultivars: Dynamics during fruit development. *Hortscience* **45,** 1150-1154.
11. Macheix, J. J., J. C. Sapis and A. Fleuriet (1991) Phenolic compounds and polyphenoloxidase in relation to browning in grapes and wines. *Crit. Rev. Food Sci. Nutr.* **30,** 441-486.
12. Waterhouse, A. L. and V. F. Laurie (2006) Oxidation of wine phenolics: A critical evaluation and hypotheses. *Am. J. Enol. Vitic.* **57,** 306-313.
13. Arzillo, M., G. Mangiapia, A. Pezzella, R. K. Heenan, A. Radulescu, L. Paduano and M. d'Ischia (2012) Eumelanin buildup on the nanoscale: Aggregate growth/assembly and visible absorption development in biomimetic 5,6-dihydroxyindole polymerization. *Biomacromolecules* **13,** 2379-2390.
14. Panzella, L., G. Gentile, G. D'Errico, N. F. Della Vecchia, M. E. Errico, A. Napolitano, C. Carfagna and M. d'Ischia (2013) Atypical structural and pi-electron features of a melanin polymer that lead to superior free-radical-scavenging properties. *Angew. Chem. Int. Ed. Engl.* **52,** 12684-12687.
15. Meredith, P. and T. Sarna (2006) The physical and chemical properties of eumelanin. *Pigm. Cell Res.* **19,** 572-594.
16. Frontana, C. and I. Gonzalez (2005) The role of intramolecular hydrogen bonding in the electrochemical behavior of hydroxy-quinones and in semiquinone stability. *J. Braz. Chem. Soc.* **16,** 299-307.
17. Tuna, D., A. Udvarhelyi, A. L. Sobolewski, W. Domcke and T. Domratcheva (2016) Onset of the electronic absorption spectra of isolated and pi-stacked oligomers of 5,6-dihydroxyindole: An ab initio study of the building blocks of eumelanin. *J. Phys. Chem. B* **120,** 3493-3502.
18. Micillo, R., L. Panzella, M. Iacomino, G. Prampolini, I. Cacelli, A. Ferretti, O. Crescenzi, K. Koike, A. Napolitano and M. d'Ischia (2017) Eumelanin broadband absorption develops from aggregation-modulated chromophore interactions under structural and redox control. *Scientific*

reports **7,** 41532.
19. Corani, A., A. Pezzella, T. Pascher, T. Gustavsson, D. Markovitsi, A. Huijser, M. d'Ischia and V. Sundstrom (2013) Excited-state proton-transfer processes of dhica resolved: From sub-picoseconds to nanoseconds. *J. Phys. Chem. Lett.* **4,** 1383-1388.
20. Corani, A., A. Huijser, T. Gustavsson, D. Markovitsi, P. A. Malmqvist, A. Pezzella, M. d'Ischia and V. Sundstrom (2014) Superior photoprotective motifs and mechanisms in eumelanins uncovered. *J. Am. Chem. Soc.* **136,** 11626-11635.
21. Gauden, M., A. Pezzella, L. Panzella, M. T. Neves-Petersen, E. Skovsen, S. B. Petersen, K. M. Mullen, A. Napolitano, M. d'Ischia and V. Sundstrom (2008) Role of solvent, ph, and molecular size in excited-state deactivation of key eumelanin building blocks: Implications for melanin pigment photostability. *J. Am. Chem. Soc.* **130,** 17038-17043.
22. Gauden, M., A. Pezzella, L. Panzella, A. Napolitano, M. d'Ischia and V. Sundstrom (2009) Ultrafast excited state dynamics of 5,6-dihydroxyindole, a key eumelanin building block: Nonradiative decay mechanism. *J. Phys. Chem. B* **113,** 12575-12580.
23. Huijser, A., A. Pezzella and V. Sundstrom (2011) Functionality of epidermal melanin pigments: Current knowledge on UV-dissipative mechanisms and research perspectives. *Phys. Chem. Chem. Phys.* **13,** 9119-9127.
24. Körner, A. and J. Pawelek (1982) Mammalian tyrosinase catalyzes three reactions in the biosynthesis of melanin. *Science* **217,** 1163-1165.
25. Horbury, M. D., L. A. Baker, W. D. Quan, J. D. Young, M. Staniforth, S. E. Greenough and V. G. Stavros (2015) Bridging the gap between the gas phase and solution phase: Solvent specific photochemistry in 4-tert-butylcatechol. *J. Phys. Chem. A* **119,** 11989-11996.
26. Yanai, T., D. P. Tew and N. C. Handy (2004) A new hybrid exchange–correlation functional using the coulomb-attenuating method (cam-b3lyp). *Chem. Phys. Lett.* **393,** 51-57.
27. Frisch, M. J., G. W. Trucks, H. B. Schlegel, G. E. Scuseria, M. A. Robb, J. R. Cheeseman, G. Scalmani, V. Barone, G. A. Petersson, H. Nakatsuji, X. Li, M. Caricato, A. V. Marenich, J. Bloino, B. G. Janesko, R. Gomperts, B. Mennucci, H. P. Hratchian, J. V. Ortiz, A. F. Izmaylov, J. L. Sonnenberg, Williams, F. Ding, F. Lipparini, F. Egidi, J. Goings, B. Peng, A. Petrone, T. Henderson, D. Ranasinghe, V. G. Zakrzewski, J. Gao, N. Rega, G. Zheng, W. Liang, M. Hada, M. Ehara, K. Toyota, R. Fukuda, J. Hasegawa, M. Ishida, T. Nakajima, Y. Honda, O. Kitao, H. Nakai, T. Vreven, K. Throssell, J. A. Montgomery Jr., J. E. Peralta, F. Ogliaro, M. J. Bearpark, J. J. Heyd, E. N. Brothers, K. N. Kudin, V. N. Staroverov, T. A. Keith, R. Kobayashi, J. Normand, K. Raghavachari, A. P. Rendell, J. C. Burant, S. S. Iyengar, J. Tomasi, M. Cossi, J. M. Millam, M. Klene, C. Adamo, R. Cammi, J. W. Ochterski, R. L. Martin, K. Morokuma, O. Farkas, J. B. Foresman and D. J. Fox (2016) Gaussian 16 rev. B.01. Wallingford, CT.
28. Aquilante, F., L. De Vico, N. Ferre, G. Ghigo, P. A. Malmqvist, P. Neogrady, T. B. Pedersen, M. Pitonak, M. Reiher, B. O. Roos, L. Serrano-Andres, M. Urban, V. Veryazov and R. Lindh (2010) Molcas 7: The next generation. *J. Comput. Chem.* **31,** 224-247.
29. Whetsel, K. B. and J. H. Lady (1970) Self-association of phenol in nonpolar solvents. In *Spectrometry of fuels*. (Edited by R. A. Friedel), pp. 259-279. Plenum Press, New York.
30. Dearden, J. C. (1963) Investigation of the self-association of phenols and anilines by ultraviolet spectroscopy. *Can. J. Chem.* **41,** 2683-2691.
31. Gerrard, D. L. and W. F. Maddams (1978) Solvent effects in u.V. Absorption spectra. I. Phenol in cyclohexane ethanol mixtures. *Spectrochim. Acta* **34A,** 1205-1211.
32. Anderson, B. D., J. H. Rytting and T. Higuchi (1979) Influence of self-association on the solubility of phenol in isooctance and cyclohexane. *J. Am. Chem. Soc.* **101,** 5194-5197.
33. Chatterley, A. S., J. D. Young, D. Townsend, J. M. Zurek, M. J. Paterson, G. M. Roberts and V. G. Stavros (2013) Manipulating dynamics with chemical structure: Probing vibrationally-enhanced tunnelling in photoexcited catechol. *Phys. Chem. Chem. Phys.* **15,** 6879-6892.
34. Kjaergaard, H. G., D. L. Howard, D. P. Schofield and T. W. Robinson (2002) Oh- and ch-stretching overtone spectra of catechol. *J. Phys. Chem. A* **106,** 258-266.

35. Davies, M. M. (1938) A note on the infra-red absorption of some phenolic compounds. *Trans. Faraday Soc.* **1938,** 1427-1429.
36. Spencer, J. N., R. A. Heckman, R. S. Harner, S. L. Shoop and K. S. Robertson (1973) Effects of the intramolecular hydrogen bond on intermolecular hydrogen bonding in hydroxybenzene-ether systems. *J. Phys. Chem.* **77,** 3103-3106.
37. Gaffney, K. J., P. H. Davis, I. R. Piletic, N. E. Levinger and M. D. Fayer (2002) Hydrogen bond dissociation and reformation in methanol oligomers following hydroxyl stretch relaxation. *J. Phys. Chem. A* **106,** 12012-12023.
38. Varfolomeev, M. A., D. I. Abaidullina, A. Z. Gainutdinova and B. N. Solomonov (2010) Ftir study of h-bonds cooperativity in complexes of 1,2-dihydroxybenzene with proton acceptors in aprotic solvents: Influence of the intramolecular hydrogen bond. *Spectrochim. Acta, Part A* **77,** 965-972.
39. Foti, M. C., L. R. C. Barclay and K. U. Ingold (2002) The role of hydrogen bonding on the h-atom-donating abilities of catechols and naphthalene diols and on a previously overlooked aspect of their infrared spectra. *J. Am. Chem. Soc.* **124,** 12881-12888.
40. Pal, S., B. Chowdhury, M. Patra, M. Maji and B. Biswas (2015) Ligand centered radical pathway in catechol oxidase activity with a trinuclear zinc-based model: Synthesis, structural characterization and luminescence properties. *Spectrochim. Acta, Part A* **144,** 148-154.
41. Albarran, G., W. Boggess, V. Rassolov and R. H. Schuler (2010) Absorption spectrum, mass spectrometric properties, and electronic structure of 1,2-benzoquinone. *J. Phys. Chem. A* **114,** 7470-7478.
42. Kumari, S., A. K. Mahato, A. Maurya, V. K. Singh, N. Kesharwani, P. Kachhap, I. O. Koshevoy and C. Haldar (2017) Syntheses and characterization of monobasic tridentate cu(ii) schiff-base complexes for efficient oxidation of 3,5-di-tert-butylcatechol and oxidative bromination of organic substrates. *New J. Chem.* **41,** 13625-13646.
43. Land, E. J. and G. Porter (1963) Primary photochemical processes in aromatic molecules. Part 7.—spectra and kinetics of some phenoxyl derivatives. *Trans. Faraday Soc.* **59,** 2016-2026.
44. Land, E. J., G. Porter and E. Strachan (1961) Primary photochemical processes in aromatic molecules. Part 6.—the absorption spectra and acidity constants of phenoxyl radicals. *Trans. Faraday Soc.* **57,** 1885-1893.
45. King, G. A., T. A. Oliver, R. N. Dixon and M. N. Ashfold (2012) Vibrational energy redistribution in catechol during ultraviolet photolysis. *Phys. Chem. Chem. Phys.* **14,** 3338-3345.
46. Harris, S. J., D. Murdock, Y. Zhang, T. A. Oliver, M. P. Grubb, A. J. Orr-Ewing, G. M. Greetham, I. P. Clark, M. Towrie, S. E. Bradforth and M. N. Ashfold (2013) Comparing molecular photofragmentation dynamics in the gas and liquid phases. *Phys. Chem. Chem. Phys.* **15,** 6567-6582.
47. Zhang, Y., T. A. A. Oliver, M. N. R. Ashfold and S. E. Bradforth (2012) Contrasting the excited state reaction pathways of phenol and para-methylthiophenol in the gas and liquid phases. *Faraday Discuss.* **157,** 141.
48. Siebbeles, L. D. A., U. Emmerichs, A. Hummel and H. J. Bakker (1997) A subpicosecond pump-probe laser study of ionization and geminate charge recombination kinetics in alkane liquids. *J. Chem. Phys.* **107,** 9339-9347.
49. Gerhards, M., W. Perl, S. Schumm, U. Henrichs, C. Jacoby and K. Kleinermanns (1996) Structure and vibrations of catechol and catechol· $H_2O(D_2O)$ in the S_0 and S_1 state. *J. Chem. Phys.* **104,** 9362-9375.
50. Young, J. D., M. Staniforth, M. J. Paterson and V. G. Stavros (2015) Torsional motion of the chromophore catechol following the absorption of ultraviolet light. *Phys. Rev. Lett.* **114,** 233001.
51. Crowell, R. A., R. Lian, M. C. Sauer, D. A. Oulianov and I. A. Shkrob (2004) Geminate recombination of hydroxyl radicals generated in 200 nm photodissociation of aqueous hydrogen peroxide. *Chem. Phys. Lett.* **383,** 481-485.
52. Elles, C. G., M. J. Cox, G. L. Barnes and F. F. Crim (2004) Recombination and reaction dynamics

following photodissociation of ch3ocl in solution. *J. Phys. Chem. A* **108,** 10973-10979.
53. Sheps, L., A. C. Crowther, C. G. Elles and F. F. Crim (2005) Recombination dynamics and hydrogen abstraction reactions of chlorine radicals in solution. *J. Phys. Chem. A* **109,** 4296-4302.
54. Stickrath, A. B., E. C. Carroll, X. Dai, D. A. Harris, A. Rury, B. Smith, K. Tang, J. Wert and R. J. Sension (2009) Solvent-dependent cage dynamics of small nonpolar radicals: Lessons from the photodissociation and geminate recombination of alkylcobalamins. *J. Phys. Chem. A* **113,** 8513-8522.
55. Giuliano, B. M., I. Reva, L. Lapinski and R. Fausto (2012) Infrared spectra and ultraviolet-tunable laser induced photochemistry of matrix-isolated phenol and phenol-d5. *J. Chem. Phys.* **136,** 024505.
56. Zimmerman, H. E. and G. Jones II (1969) The photochemistry of a cyclohexadienone structurally incapable of rearrangement. Exploratory and mechanistic organic photochemistry. Xlvii. *J. Am. Chem. Soc.* **92,** 2753-2761.
57. Derkosch, J. and W. Kaltenegger (1959) Die IR-spektren von derivaten der cyclohexadienone. *Monatsh. Chem.* **90,** 877-884.
58. Mvula, E., M. N. Schuchmann and C. von Sonntag (2001) Reactions of phenol-oh-adduct radicals. Phenoxyl radical formation by water elimination vs. Oxidation by dioxygen. *J. Chem. Soc., Perkin Trans. 2***,** 264-268.
59. Adams, G. E. and B. D. Michael (1967) Pulsed radiolysis of benzoquinone and hydroquinone. *Trans. Faraday Soc.* **63,** 1171-1180.
60. Richter, H. W. (1979) Pulse radiolysis f 4-tert-butyl-1,2-dihydroxybenzene and 4-tert-butyl-1,2-quinone. *J. Phys. Chem.* **83,** 1123-1129.
61. Quinkert, G. (2009) Photochemistry of linearly conjugated cyclohexadienones in solution. *Pure Appl. Chem.* **33,** 285-316.
62. Bloom, S. M. (1959) An acid stable cyclohexadienone. *Tetrahedron Lett.* **1,** 7-9.
63. Greenough, S. E., M. D. Horbury, J. O. Thompson, G. M. Roberts, T. N. Karsili, B. Marchetti, D. Townsend and V. G. Stavros (2014) Solvent induced conformer specific photochemistry of guaiacol. *Phys. Chem. Chem. Phys.* **16,** 16187-16195.
64. Weichert, A., C. Tiehn and B. Brutschy (2001) High-resolution rotational coherence spectroscopy of the phenol dimer. *J. Phys. Chem. A* **105,** 5679-5691.
65. Koch, M., R. Letrun and E. Vauthey (2014) Exciplex formation in bimolecular photoinduced electron-transfer investigated by ultrafast time-resolved infrared spectroscopy. *J. Am. Chem. Soc.* **136,** 4066-4074.
66. Koch, M., G. Licari and E. Vauthey (2015) Bimodal exciplex formation in bimolecular photoinduced electron transfer revealed by ultrafast time-resolved infrared absorption. *The journal of physical chemistry. B* **119,** 11846-11857.
67. Kennehan, E. R., C. Grieco, A. N. Brigeman, G. S. Doucette, A. Rimshaw, K. Bisgaier, N. C. Giebink and J. B. Asbury (2017) Using molecular vibrations to probe exciton delocalization in films of perylene diimides with ultrafast mid-IR spectroscopy. *Physical chemistry chemical physics : PCCP* **19,** 24829-24839.
68. Poterya, V., L. Sistik, P. Slavicek and M. Farnik (2012) Hydrogen bond dynamics in the excited states: Photodissociation of phenol in clusters. *Phys. Chem. Chem. Phys.* **14,** 8936-8944.
69. Chipman, D. M. (2006) Stretching of hydrogen-bonded oh in the lowest singlet excited electronic state of water dimer. *J. Chem. Phys.* **124,** 044305.
70. Nighswander-Rempel, S. P., J. Riesz, J. Gilmore, J. P. Bothma and P. Meredith (2005) Quantitative fluorescence excitation spectra of synthetic eumelanin. *J. Phys. Chem. B* **109,** 20629-20635.

Table 1. Excited state O-H dissociation and H-atom transfer barriers for monomers and dimers of 4-tBuC determined using TD-CAM-B3LYP/6-311g**.

System	Reaction	Barrier
Monomer	H Dissociation (free OH)	0.10 eV
	H Transfer (intramolecular)	0.74 eV
Dimer	H Dissociation (free OH)	0.11 eV
	H Transfer (intermolecular)	0.51 eV

Figure and Scheme Captions

Scheme 1. Molecules discussed in the text.

Figure 1. (a) Normalized UV absorption spectra featuring the $S_0 \rightarrow S_1$ transition, and **(b)** FTIR spectra of 4-*t*-butylcatechol (4-tBuC, structure shown in **a**) in cyclohexane at various concentrations (arrows indicate increasing concentration). The monomer OH bands are labeled as "b" (intramolecularly hydrogen bonded) and "f" (free). **(c)** Fractional populations of monomers and aggregates deduced from the FTIR spectra. **(d)** List of assigned O-H stretching frequencies. **(e)** Possible hydrogen-bonding patterns discussed in the text. The O-H bonds are color-coded to match the assignments in **(d)**.

Figure 2. Transient UV-Vis spectroscopy of solutions of t-butylcatechol in cyclohexane predominantly comprised of either **(a)** monomers (5 mM) or **(b)** aggregates (75 mM). All samples were measured using ~400 μJ/cm^2 (absorbed) excitation at 265 nm. The path lengths for the 5 mM and 75 mM samples were 500 μm and 100 μm, respectively. Spectra are presented for several time delay ranges. The black trace in **(a)** is the spectrum of neat cyclohexane averaged between 100 and 250 ps, measured under identical conditions as the 5 mM sample.

Figure 3. Spectrally integrated transient absorption kinetics for **(a)** 5 mM (monomer) and (b) 75 mM (primarily aggregate) solutions of 4-tBuC in cyclohexane excited at 265 nm.

Figure 4. Time-resolved vibrational spectroscopy of solutions of 4-*t*-butylcatechol in cyclohexane predominantly comprising of either **(a)** monomers (10 mM) or **(c)** aggregates (75 mM). All samples were measured using ~1.6 mJ/cm^2 (absorbed) excitation at 265 nm. The signal arising from the neat solvent was subtracted as discussed in the Supporting Information. The path lengths for the 5 mM and 75 mM samples were 500 µm and 100 µm, respectively. The colored rectangles show spectral ranges that were averaged over to obtain the kinetics traces shown in **Figure 5**. The inverted FTIR spectra for the 10 mM and 75 mM samples are shown in **(b)** and **(d)**, respectively.

Figure 5. Kinetic decays of key transient features in the time-resolved vibrational spectrum of **(a)** 10 mM and **(b)** 75 mM solutions of 4-tBuC in cyclohexane following 265 nm excitation. The kinetic decays shown in red were obtained by averaging the signals recorded around 1341 cm^{-1} and 1406 cm^{-1}. The kinetic decays shown in blue were obtained by averaging the signals recorded around 1650cm^{-1}. **(c)** Ground state bleach (GSB) kinetics obtained by integrating the vibrational bleach signal around 1290 cm^{-1}.

Figure 6. Absorption spectra of **(a)** 5 mM and **(b)** 75 mM solutions of 4-tBuC in cyclohexane during UV irradiation for the indicated times. The quantum yields of the quinone photoproducts are indicated.

Figure 7. Optimized 4-tBuC **(a)** monomer and **(b)** dimer structures (CAM-B3LYP/6-311G**). Various O---H distances are displayed in Å for the ground-state and excited-state minima (plain text and italics, respectively).

Scheme 2. Proposed kinetic models for monomers and aggregates of 4-tBuC. ^{1}(4-tBuC)$^*_{relax}$ represents a structurally relaxed S_1 state. The time constants shown are from target analysis of the transient UV-Vis data.

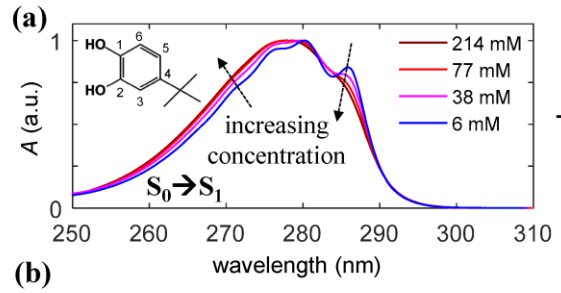

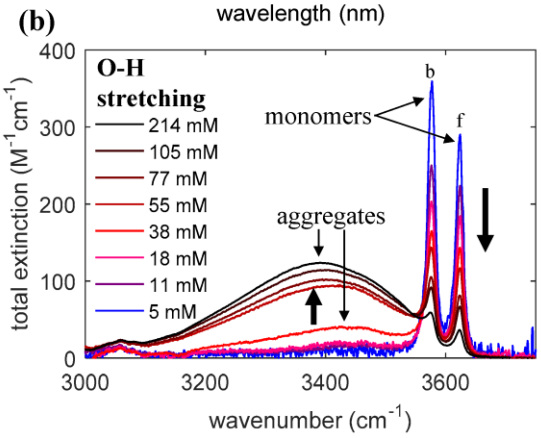

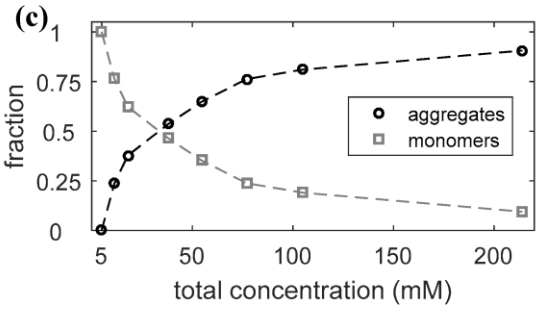

(d)

center frequency (cm^{-1})	assignment	type
3624	free OH (f)	"monomer"
3576	intramolecularly-bonded OH (b)	"monomer"
3440, 3400	intermolecularly-bonded OH	"aggregate"

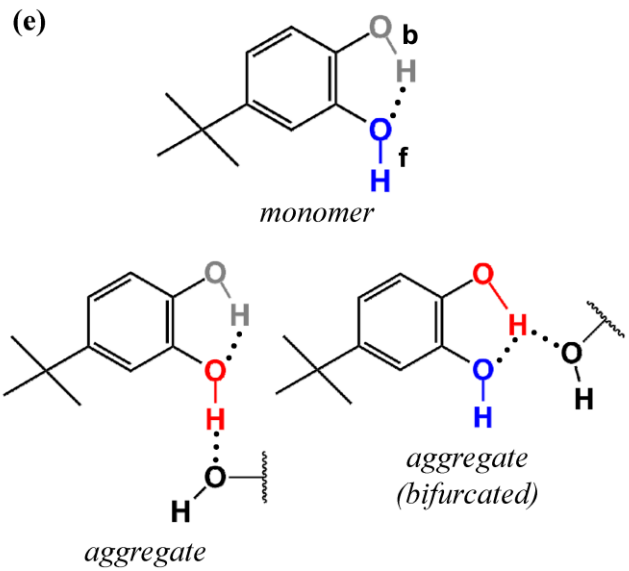

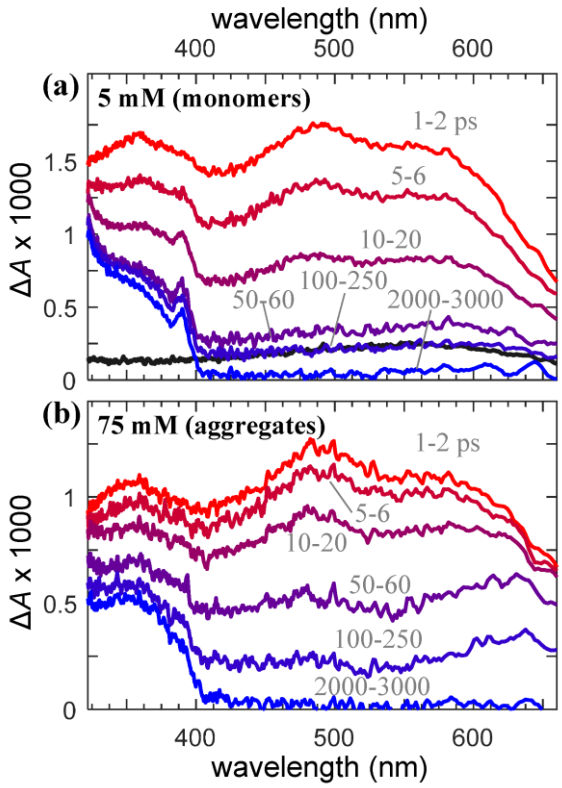

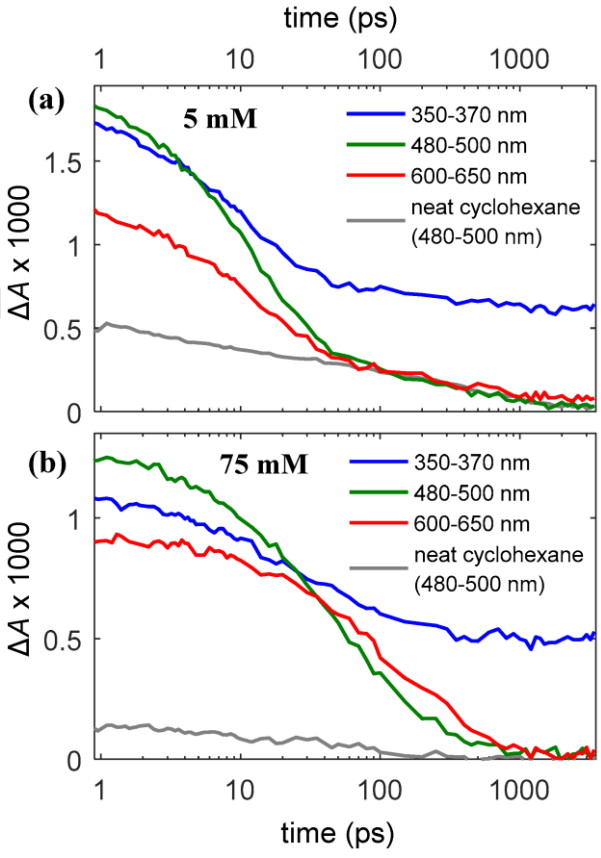

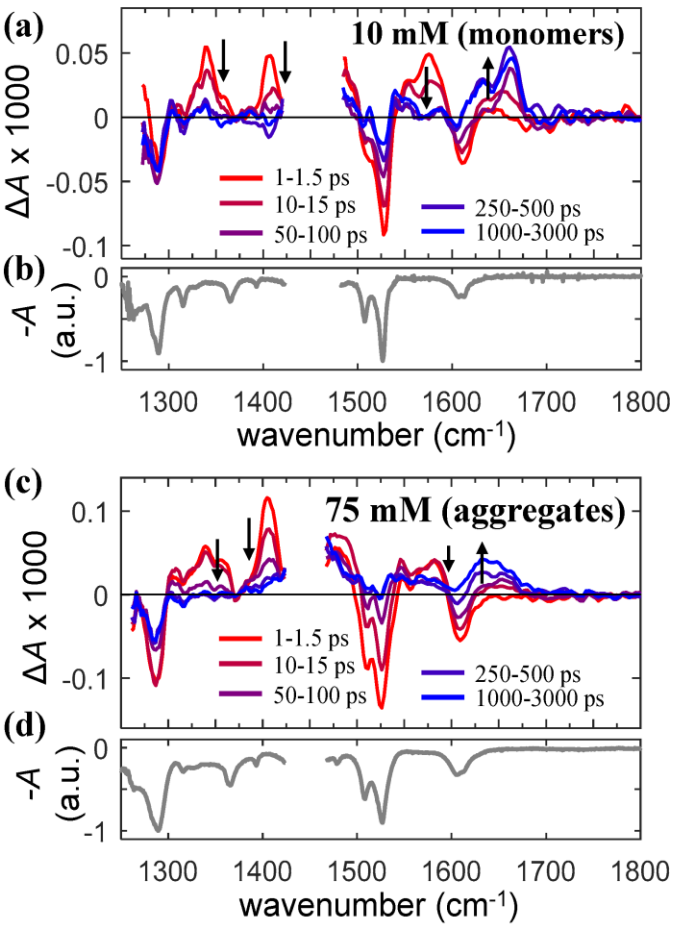

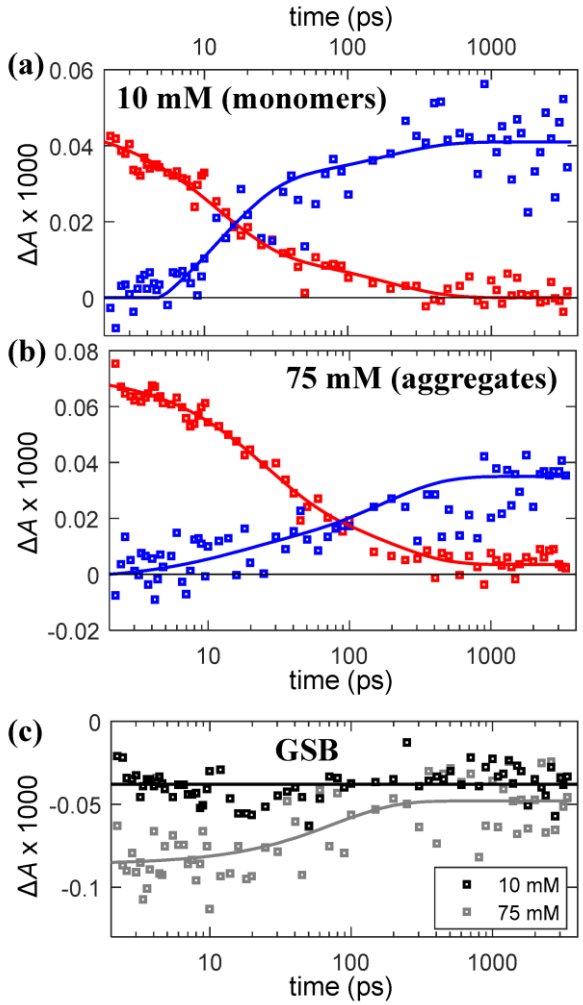

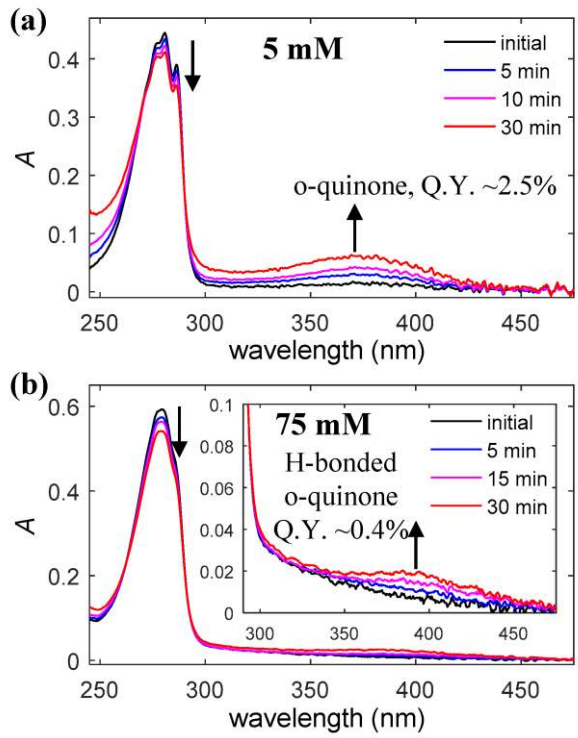

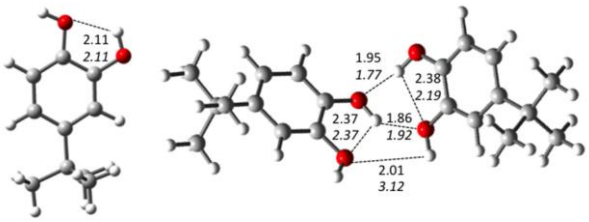

(a) (b)